Journal of Engineering Mathematics **49:** 289–304, 2004.

Elastostatic Green's function for advanced materials subject to surface loading

V.K. TEWARY
Materials Reliability Division, National Institute of Standards and Technology, Boulder, CO 80305, U.S.A.

Received 20 December 2003; accepted in revised form 24 March 2004

Abstract. This paper gives a brief review of the Green's function method for solution of the general three-dimensional Boussinesq problem for advanced materials that are highly anisotropic. The Boussinesq problem refers to calculation of stress and/or strain fields in semi-infinite solids, subject to surface loading by solving the equations of elastostatic equilibrium. Analytical and semi-analytical expressions are derived for the elastostatic Green's functions based upon the delta-function representation developed earlier. The Green's function provides a computationally efficient method for solving the anisotropic Boussinesq problem. The Green's function should be useful for modeling physical systems of topical interest such as nanostructures in semiconductors, interpretation of nanoindentation measurements, and application to the boundary-element method of stress analysis of advanced materials. Numerical results for displacement and stress fields are presented for carbon-fiber composites having general orthotropic, tetrahedral, and hexagonal symmetries, and single-crystal silicon having cubic symmetry.

Key words: Boussinesq problem, carbon-fiber composite, elastic anisotropy, elastostatic Green's functions, silicon

1. Introduction

With current developments in nanotechnology, there is a strong interest in computationally efficient techniques for calculation of stress and/or strain fields in advanced materials such as single-crystal semiconductors and composites that are, in general, highly anisotropic. For example, a nanostructure such as a quantum dot growing inside or on the surface of a semiconductor induces a strain field in the entire solid. Growth and stability of quantum dots and their arrays depend crucially on the induced strain field [1, Chapter 5]. Similarly, the interpretation of nanoindentation measurements requires knowledge of the strain field caused by the nanoindenter at the surface [2]. Even bulk structural materials like fiber composites are highly anisotropic and new methods are required for their stress analysis when subjected to surface or internal loads. Elastic Green's functions along with the boundary-element method (BEM) provide a powerful technique [3, Chapters 3, 5] for solving such problems.

In addition to stress/strain analysis, elastic Green's functions are useful for characterizing solids and calculating their effective elastic constants (see, for example, [4, 5]). Elastic Green's functions for anisotropic single crystals are needed in the study of lattice defects using continuum theory (see, for example, [6, 7], [8, Chapter 13]) and for multiscale modeling [9] of defects and nanostructures. For an excellent review of the work on the continuum model of anisotropic solids and other references, see the treatise by Ting [10, Chapter 8].

Green's functions are most useful for solving boundary-value problems [11, Chapter 1]. The chief advantage of the Green's function method is that it is a characteristic of the material, and its geometry and structure, but is independent of the applied load. Once the Green's function is calculated and stored for a particular material, it can be used for different loads

on the same material. Different types of Green's functions are defined for different classes of problems. Our interest in this paper is confined to elastostatic Green's functions that are used to calculate elastic displacement fields and related quantities such as stresses and strains in the continuum model of solids. For brevity, henceforth we will omit the prefix elastostatic and refer to the elastostatic Green's function as GF.

The calculation and properties of GF for an infinite solid have been described in many text books and review articles (see, for example, [10, Chapter 8] and [11, Chapter 1], which give other references). Powerful methods have been developed for calculating GFs for anisotropic infinite solids [12–19]. Wang and Achenbach [20–22] have developed a Radon-transform [23] method for calculating GFs. Ting and Lee [12] have calculated GFs in terms of the Stroh roots of the Christoffel equations. However, a real material is not infinite. It has free surfaces and may have other discontinuities such as interfaces and structural defects such as dislocations, cracks, etc., which can be incorporated into the analysis by specifying suitable boundary conditions. The infinite-solid GFs along with the BEM are used for solving such boundary-value problems in real materials. The BEM is a powerful numerical technique and can be applied to boundaries of arbitrary shapes. It is, however, computationally intensive. In case of geometrically simple boundaries, such as a free planar surface, it is possible to obtain the GF analytically or semi-analytically, which is computationally more efficient.

In many real applications, it is adequate to include the effect of a single free surface and neglect the effect of other free surfaces in the solid. Examples include the growth of quantum dots at or near a free surface and nanoindentation measurements where the other free surfaces are far enough. If needed, the effect of other free surfaces can be included by using the BEM starting from the GF for a single free surface. This should be computationally more efficient than using the infinite-solid GF in BEM.

There are two classes of problems [24, Chapter 10] for analysis of strains in solids with a single free surface: the Mindlin problem and the Boussinesq problem. In the Mindlin problem, the solid is subjected to a body force from inside. One important application of these Green's functions is in modeling buried quantum dots [25] in semiconductors. In contrast, in the Boussinesq problem, the force is applied at the surface of the solid from outside. The GF for the Boussinesq problem is applicable to problems involving surface loading such as in nanoindentation experiments or growth of surface quantum dots.

The Mindlin problem has been elegantly analyzed in a recent paper by Pan [26]. He has also discussed the limiting case of the Mindlin problem when the point where the force is applied approaches the free surface from inside. The GF for the Mindlin problem has also been derived by Walker [27] using the Fourier-integral representation. Detailed numerical calculations on the Mindlin problem with application to embedded quantum dots are already available in the literature [25, 28]. In this paper, therefore, we will not discuss the Mindlin GFs and confine ourselves to the GF for the Boussinesq problem.

The solution of the isotropic Boussinesq problem has been given in, for example, [24]. Transverse isotropic and axially symmetric cases have been considered in references [29–38]. Wang *et al.* [39] have calculated displacements and stresses in an inhomogeneous transversely isotropic semi-infinite solid subject to a vertical load. The two-dimensional (2D) problem of a line force loading on an anisotropic semi-infinite solid has been solved by Barnett and Lothe [40], who have also obtained the surface displacements due to a point force on the surface. Numerical solutions for the anisotropic Boussinesq problem using BEM and other purely numerical methods have been reported in many papers such as [41–44]. A general solution of the Boussinesq problem in the Fourier space was given by Willis [45] without the inversion

of the Fourier transform. A solution for some special cases of the Boussinesq problem has been given by Svelko (quoted in [45]). In a very interesting paper, Every [46] has used a ring integral expression for the GF for the Boussinesq problem by taking the zero-frequency limit of the elastodynamic GF in the Fourier representation.

In this paper we describe the delta-function representation of the GF for the Boussinesq problem. We derive a semi-analytic expression for the GF that gives the displacement and stress fields in 3D anisotropic semi-infinite solids subject to a point force applied on the surface. For the purpose of illustration, we present numerical results for the stress and displacement fields in the following materials of practical interest: carbon-fiber composites having general orthotropic, tetrahedral, or hexagonal symmetries, and single-crystal silicon having cubic symmetry.

The delta-function representation of the GF is a modified form of the one developed earlier [47] in slowness space for the elastodynamic case. It gives a semi-analytic expression for the GF that is computationally convenient for anisotropic elastostatic applications. Analytical expressions are obtained for even components of the GF at the free surface. In general, only a 1D integral needs to be evaluated numerically over a finite interval. Our solution requires the roots of at most a 6-degree polynomial equation, as in Stroh's method. In symmetry planes, only the roots of a cubic equation are needed, which are obtained analytically.

In the Boussinesq problem, only the homogeneous solution of the Christoffel equation is needed. In the GF method, the homogeneous solution is usually obtained by introducing image sources or fields [48, Chapter 7] or by applying virtual forces at the boundaries [49, 50]. The boundary conditions are then satisfied either analytically [49–51], or numerically, as in the BEM [3, 52, 53]. In the delta-function representation, we obtain the homogeneous solution directly by using the imaginary part of the complex GF in the reciprocal space. One advantage of this method is that the location of virtual forces does not need to be specified. Although the computational efficiency of the delta-function representation is comparable to other methods [26, 45, 46], it appears to be more convenient for multiscale modeling [9] of nanostructures. This is because the virtual force introduced for satisfying the boundary conditions is directly related to the Kanzaki force [9] in the multiscale formulation.

The general solution and the GF of the Boussinesq problem are given in Section 2. Numerical results are presented in Section 3 for semi-infinite single-crystal cubic silicon, and hexagonal, tetragonal, and orthotropic (PEEK) carbon-fiber composites. The conclusions are summarized in Section 4.

2. General solution of the Boussinesq problem

We denote the space variable by $\boldsymbol{x}$. The Cartesian components will be denoted by indices i, j, k, etc., which assume the values 1, 2, or 3, corresponding to x-, y-, and z-coordinates. For notational convenience, we introduce a 2D vector $\boldsymbol{X}$ in the x-y subspace of the 3D vector $\boldsymbol{x}$ such that $X_1 = x_1$ and $X_2 = x_2$. Obviously $\boldsymbol{x}$ can be written as (x_1, x_2, x_3) or $(\boldsymbol{X},x_3)$. We also define a conjugate 3D vector $\boldsymbol{q}$ in the reciprocal space such that $\boldsymbol{q}\cdot\boldsymbol{x}$ is dimensionless. Note the difference with the elastodynamic case [47], where $\boldsymbol{q}\cdot\boldsymbol{x}$ has the dimensions of time and $\boldsymbol{q}$ is a slowness vector. Corresponding to X in the x space, we define a 2D vector $\boldsymbol{Q}$ in the reciprocal space such that $Q_1 = q_1$ and $Q_2 = q_2$, and $\boldsymbol{q} = (q_1, q_2, q_3)$ or $(\boldsymbol{Q},q_3)$. Henceforth, summation over repeated Roman indices is implied unless stated otherwise.

The Boussinesq problem is to determine the displacement field and stress field in a half-space solid subject to a concentrated load at the free surface. The solid is assumed to have no body force. The displacement field satisfies the homogeneous Christoffel equation

$$L_{ij}u_j(\boldsymbol{x}) = 0, \tag{2.1}$$

where

$$L_{ij} = c_{ikjl}\partial^2/\partial x_k \partial x_l, \tag{2.2}$$

and $\boldsymbol{c}$ is the fourth-rank elastic-constant tensor. We choose a frame of reference in which the origin and the x- and y-axes are on the free surface and the positive z-axis points into the solid. If the point load is applied at the origin of coordinates, the boundary conditions are prescribed by

$$\tau_{i3}(\boldsymbol{X}) = \eta_i \delta(\boldsymbol{X}) \quad (x_3 = 0), \tag{2.3}$$

where $\boldsymbol{\tau}$ denotes the stress tensor, δ denotes the Dirac delta function and $\boldsymbol{\eta}$ is a constant vector representing the strength of the applied load. The boundary condition given by (2.3) specifies the tractions to be 0 everywhere on the free surface except at the point where the load is applied. If we replace $\boldsymbol{\eta}$ by a unit vector, the displacement field would give the Green's function. By definition

$$\tau_{i3}(\boldsymbol{x}) = c_{i3jk}\partial u_j(\boldsymbol{x})/\partial x_k. \tag{2.4}$$

In the Green's function method, it is conventional [49, 50] to apply virtual forces (or image forces) at the boundaries of the solid in order to satisfy the boundary conditions. The location of the virtual forces at the boundary ensures that the displacement field satisfies the homogeneous equation (2.1) in the bulk of the solid. In this paper we use the imaginary part of the Green's function in reciprocal space (see 2.6 below) that gives the homogeneous solution without any need to specify the location of the virtual forces.

In an earlier paper [47], we described the delta-function representation of the elastodynamic Green's function. In the static limit, we use the following modified form for the Green's function $\boldsymbol{G}_H$ that gives a solution of (2.1):

$$\boldsymbol{G}_H(\boldsymbol{x}) = K\Im\mathrm{m}\int \boldsymbol{G}_I(\boldsymbol{q})\Delta(\boldsymbol{q}\cdot\boldsymbol{x})\mathrm{d}\boldsymbol{q}, \tag{2.5}$$

where

$$\boldsymbol{G}_I(\boldsymbol{q}) = \mathrm{Lim}_{\varepsilon\to+0}\Im\mathrm{m}[\boldsymbol{\Lambda}(\boldsymbol{q}) - \mathrm{i}\varepsilon\boldsymbol{I}]^{-1}, \tag{2.6}$$

$$\Lambda_{ij}(\boldsymbol{q}) = c_{ikjl}q_k q_l, \tag{2.7}$$

$$\Delta(z) = (-1/\pi)\mathrm{Lim}_{\varepsilon\to+0}[z + \mathrm{i}\varepsilon]^{-1}, \tag{2.8}$$

K is an arbitrary constant, $\boldsymbol{I}$ is the 3×3 unit matrix, $\mathrm{i} = \sqrt{(-1)}$, and $\Im\mathrm{m}z > 0$. The integration in q-space in (2.5) is over a surface so that only two of the three components of $\boldsymbol{q}$ are independent. The actual surface over which the integration is to be carried out depends upon the application, and will be specified later. In (2.8), z is a real or complex scalar. For real z, the imaginary part of $\Delta(z)$ is given by the well known identity

$$\Im\mathrm{m}\Delta(\mathrm{z}) = \delta(\mathrm{z}). \tag{2.9}$$

The function $\delta(z)$ in (2.9) is equivalent to the $t = 0$ limit of the Radon representation discussed by Willis [23], and Wang and Achenbach [21]. Here it restricts the q-vector in a plane normal to $\boldsymbol{x}$. Our method thus becomes similar to that used by Barnett [13], and Ting and Lee [12] for calculating the free-space Green's function for infinite solids without any boundary conditions. The main difference is that they have used the real part of (2.6), whereas we use its imaginary part. We need the imaginary part here because our objective is to solve the homogeneous Christoffel equation.

We identify $\boldsymbol{\Lambda}(\boldsymbol{q})$ as the Christoffel matrix and $\boldsymbol{G_I(q)}$ as the imaginary part of the Green's function in the reciprocal space. They are 3×3 matrices. Using the eigenvector representation of a matrix, we can write

$$\boldsymbol{\Lambda}_{ij}(\boldsymbol{q}) = \sum_s e_{si}(\boldsymbol{q}) e_{sj}(\boldsymbol{q}) E_s(\boldsymbol{q}), \tag{2.10}$$

where $\boldsymbol{e}_s$ $(\boldsymbol{q})$ $(s = 1, 2, 3)$ and $E_s(\boldsymbol{q})$ are, respectively, the orthonormal eigenvectors and eigenvalues of $\boldsymbol{\Lambda}(\boldsymbol{q})$. From (2.10), using the orthonormality of the eigenvectors, we have

$$[\boldsymbol{\Lambda}(\boldsymbol{q}) - \mathrm{i}\varepsilon\mathbf{I}]^{-1}_{ij} = \sum_s e_{si}(\boldsymbol{q}) e_{sj}(\boldsymbol{q}) [E_s(\boldsymbol{q}) - \mathrm{i}\varepsilon]^{-1}. \tag{2.11}$$

For an elastically stable solid $E_s(\boldsymbol{q})$ are real. Hence, using (2.9), we obtain from (2.6),

$$\boldsymbol{G}_I(\boldsymbol{q}) = \pi \sum_s e_{si}(\boldsymbol{q}) e_{sj}(\boldsymbol{q}) \delta[E_s(\boldsymbol{q})]. \tag{2.12}$$

As in Stroh's method, (2.12) requires computation of the eigenvectors and eigenvalues of $\boldsymbol{\Lambda}(\boldsymbol{q})$. We write it in the following alternative form that we use for actual computations:

$$\boldsymbol{G}_I(\boldsymbol{q}) = \mathbf{M}(\boldsymbol{q}) \delta[D(\boldsymbol{q})], \tag{2.13}$$

where $\boldsymbol{M(q)}$ is the matrix of cofactors of $\boldsymbol{\Lambda}(\boldsymbol{q})$, and $D(\boldsymbol{q})$ is the determinant of $\boldsymbol{\Lambda}(\boldsymbol{q})$. The constant factors on the right side of (2.13) can be absorbed in K in (2.5).

Since $z\delta(z) = 0$ for any real z, (2.10) and (2.12) or (2.13) show that $\boldsymbol{\Lambda}(\boldsymbol{q})\boldsymbol{G}_I(\boldsymbol{q}) = 0$ for all values of $\boldsymbol{q}$. Hence, the solution of (2.1) (homogeneous solution) can be written as

$$\boldsymbol{u(x)} = \Im\mathfrak{m} \int \boldsymbol{G}_I(\mathbf{q}) \boldsymbol{f(Q)} \Delta(\boldsymbol{q}\cdot\boldsymbol{x}) \mathrm{d}\boldsymbol{q}, \tag{2.14}$$

where $\boldsymbol{f(Q)}$, the virtual force, is an arbitrary but integrable vector in q-space which does not depend upon q_3. We have absorbed the constant K of (2.5) in $\boldsymbol{f}$. We will allow $\boldsymbol{f}$ to be complex. We will determine the virtual force by imposing the boundary conditions. The virtual force can be obtained analytically for simple geometrical shapes as in the present case. In other cases the virtual force has to be obtained numerically, as in the BEM.

The integration over $\boldsymbol{q}$ in (2.14) is carried out over a surface in q-space so only 2 of the 3 components of $\boldsymbol{q}$ are independent. Since $\boldsymbol{G}_I(\boldsymbol{q})$ contains a delta function of the eigenvalues (or the determinant) of the Christoffel matrix, we can easily carry out the integration over one component of $\boldsymbol{q}$. We choose this component to be q_3 and do not restrict it to the real axis. The integral is given in Appendix A. The resulting $\boldsymbol{q}\cdot\boldsymbol{x}$ is in general complex.

We now proceed to determine $\boldsymbol{f(Q)}$ by imposing the boundary conditions on the homogeneous solution. From (2.4) and (2.14)

$$\boldsymbol{T(x)} = \Im\mathfrak{m} \int \boldsymbol{S(q)} \boldsymbol{G}_I(\boldsymbol{q}) \boldsymbol{f(Q)} \Delta'(\boldsymbol{q}\cdot\boldsymbol{x}) \mathrm{d}\boldsymbol{q}, \tag{2.15}$$

where $\boldsymbol{T(x)}$ is the traction vector with components $T_i = \tau_{i3}$, the prime over Δ denotes its derivative with respect to its argument, and the elements of the 3×3 matrix $\boldsymbol{S(q)}$ are

$$S_{ij}(\boldsymbol{q}) = c_{i3jk}\, q_k. \tag{2.16}$$

The integration in (2.14) and (2.15) over q_3 is done in the complex plane as shown in Appendix A. The integration over q_1 and q_2 is done over a unit circle as given below:

$$q_1 = Q_1 = \cos(\theta);\ q_2 = Q_2 = \sin(\theta);\ \mathrm{d}\boldsymbol{q} = \mathrm{d}\theta \mathrm{d}q_3. \tag{2.17}$$

From (2.3) and (2.15) at $x_3 = 0$, we obtain the following integral equation for the determination of $\boldsymbol{f(Q)}$:

$$\Im\mathfrak{m} \int_0^{2\pi} \boldsymbol{s(Q)f(Q)}\Delta'(\boldsymbol{Q}\cdot\boldsymbol{X})\mathrm{d}\theta = \boldsymbol{\eta}\delta(\boldsymbol{X}), \tag{2.18}$$

where

$$\boldsymbol{s(Q)} = \int_C \boldsymbol{S(q)G}_I\boldsymbol{(q)}\mathrm{d}q_3, \tag{2.19}$$

and the contour C for integration over q_3 is defined in Appendix A. It gives

$$\boldsymbol{s(Q)} = \sum_m \boldsymbol{S}(\boldsymbol{Q}, q_{3m})\boldsymbol{M}(\boldsymbol{Q}, q_{3m})W_m. \tag{2.20}$$

The virtual force $\boldsymbol{f}$ depends only upon $\boldsymbol{Q}$ and not on q_3. Using (B.4) of Appendix B, we may write the solution of (2.18) as

$$\boldsymbol{f(Q)} = (1/4\pi\mathrm{i})[\boldsymbol{s(Q)}]^{-1}\boldsymbol{\eta}. \tag{2.21}$$

The displacement field for the Boussinesq problem is given by (2.14). The integration in (2.14) is over two variables – q_3 and θ. The integral over q_3 is done analytically as given in Appendix A. The result is

$$\boldsymbol{u}_B\boldsymbol{(x)} = \Im\mathfrak{m} \sum_m \int_0^{2\pi} \boldsymbol{M}(\boldsymbol{Q}, q_{3m})\boldsymbol{f(Q)}W_m\, \Delta(\boldsymbol{Q}\cdot\boldsymbol{X} + q_{3m}x_3)\mathrm{d}\theta, \tag{2.22}$$

where $\boldsymbol{f(Q)}$ is given by (2.21). In general q_{3m} are complex. The integration over θ in (2.22) has to be done numerically. Note that the displacement field varies as $1/x$, where x is the magnitude of $\boldsymbol{x}$.

Finally, the Green's function for the Boussinesq problem, that is, the displacement due to a unit force on the surface, is then given by

$$\boldsymbol{G}_B\boldsymbol{(x)} = \Im\mathfrak{m} \sum_m \int_0^{2\pi} \boldsymbol{P}_m(\boldsymbol{Q})\Delta(\boldsymbol{Q}\cdot\boldsymbol{X} + q_{3m}x_3)\mathrm{d}\theta, \tag{2.23}$$

where

$$\boldsymbol{P}_m(\boldsymbol{Q}) = (1/2\pi\mathrm{i})\boldsymbol{M}(\boldsymbol{Q}, q_{3m})[\boldsymbol{s(Q)}]^{-1}W_m \tag{2.24}$$

is a 3×3 matrix.

We consider the special case of the displacement at the free surface. At $x_3 = 0$, the argument of Δ in (2.23) is real and $\boldsymbol{x} = \boldsymbol{X}$ is on the free surface. In this case the integration of those components of $\boldsymbol{P}_m(\boldsymbol{Q})$ that are even functions of Q_1 and Q_2 is considerably simplified. We write the integral in (2.23) as a sum of integrals in the intervals from 0 to π and from π to 2π. Since $\boldsymbol{Q}$ in the latter interval is $-\boldsymbol{Q}$ of the first, we can write

$$\boldsymbol{G}_B(\boldsymbol{X}) = \mathfrak{Im} \int_0^{\pi} [\boldsymbol{P}(\boldsymbol{Q})\Delta(\boldsymbol{Q}\cdot\boldsymbol{X}) + \boldsymbol{P}(-\boldsymbol{Q})\Delta(-\boldsymbol{Q}\cdot\boldsymbol{X})]\mathrm{d}\theta, \tag{2.25}$$

where

$$\boldsymbol{P}(\boldsymbol{Q}) = \sum_m \boldsymbol{P}_m(\boldsymbol{Q}). \tag{2.26}$$

Using (2.8) and (2.9), we obtain the following simple expression for the even components of the Green's function at the free surface

$$\boldsymbol{G}_{Bij}(\mathbf{X}) = \mathfrak{Re} \int_0^{\pi} \boldsymbol{P}_{ij}(\boldsymbol{Q})\delta(\boldsymbol{Q}\cdot\boldsymbol{X})\mathrm{d}\theta, \tag{2.27}$$

when

$$\boldsymbol{P}_{ij}(\boldsymbol{Q}) = \boldsymbol{P}_{ij}(-\boldsymbol{Q}), \tag{2.28}$$

which implies $\boldsymbol{G}(-\boldsymbol{X}) = \boldsymbol{G}(\boldsymbol{X})$. In such cases the integral over θ can also be done analytically simply by using the property of the delta function as given below:

$$\delta(\boldsymbol{Q}\cdot\boldsymbol{X}) = (1/X)\delta[\cos(\theta - \alpha)], \tag{2.29}$$

where $X \neq 0$ is the magnitude of $\boldsymbol{X}$ and α is its angle with the x-axis. This gives

$$\theta = \alpha + \pi/2 \quad or \quad \theta = \alpha + 3\pi/2. \tag{2.30}$$

Substituting for θ from (2.30) in the integrand in (2.27) gives an analytical expression for the displacement field. Equation (2.23) is similar to that derived independently by Svelko (quoted in [45]) and Every [46].

Proceeding as given above, we obtain the following for the traction field at $\boldsymbol{x}$:

$$\boldsymbol{T}_B(\boldsymbol{x}) = \mathfrak{Im} \sum_m \int_0^{2\pi} \boldsymbol{S}(\boldsymbol{Q}, q_{3m})\boldsymbol{P}_m(\boldsymbol{Q})\Delta'(\boldsymbol{Q}\cdot\boldsymbol{X} + q_{3m}x_3)\mathrm{d}\theta. \tag{2.31}$$

Equation (2.31) gives the stress component $\tau_{i3}(\boldsymbol{x})$. It is 0 at $x_3 = 0$ as required by the boundary condition. The other components of the stress vector can be obtained in an analogous manner.

3. Results

We calculate the displacement and the stress field in some semi-infinite solids subjected to a point load by using the formulas given in the previous section. We report numerical results for a general orthotropic fiber composite PEEK (poly-ether-ether-ketone), that has 9 elastic constants, tetragonal carbon-fiber composite (6 elastic constants), hexagonal carbon-fiber composite (5 elastic constants), and single crystal cubic silicon (3 elastic constants.

Green's functions for all these solids can be derived from the Christoffel matrix for a general orthotropic solid [54] by imposing relationships between the elastic constants as given below for each symmetry.

We write the determinant of the Christoffel matrix in each case as a polynomial in q_3 and equate it to zero with the constraint $q_1^2 + q_2^2 = 1$. For the symmetries considered here, this gives us a cubic equation in q_3^2. The roots of the cubic equation are obtained analytically. As given at the end of Appendix A, we choose three roots with positive imaginary parts. We assume that the applied force is normal to the free surface, which is taken to be the xy plane; that is $\boldsymbol{\eta} = (0, 0, \eta_3)$. In each case we present only the z-component of the displacement field. We assume units such that $c_{44} = \eta_3 = 1$. To get the result in practical units, multiply the displacement by $\eta_3/(ac_{44})$ and the stress by η_3/a^2 where η_3 is the actual force and a is the unit of length used for $\boldsymbol{x}$. Results for an arbitrary direction of loading can be obtained by taking appropriate direction of $\boldsymbol{\eta}$. For example, horizontal loading corresponds to $\boldsymbol{\eta} = (\eta_1, 0, 0)$ or $\boldsymbol{\eta} = (0, \eta_2, 0)$.

3.1. General orthotropic fiber composite – PEEK (poly-ether-ether-ketone)

We use the following values of the elastic constants for PEEK, which are given by Kim *et al.* [55]. The values are in units of c_{44} (= 22·3 GPa).

$$c_{11} = 12{\cdot}79,\ c_{22} = 6{\cdot}82,\ c_{33} = 4{\cdot}78,\ c_{55} = 1{\cdot}13,\ c_{66} = 2{\cdot}56,$$
$$c_{12} = 3{\cdot}45,\ c_{13} = 2{\cdot}69,\ c_{23} = 3{\cdot}43,\ \text{and}\ c_{44} = 1.$$

Figure 1 show the displacement field as a function of α for points $(\cos\alpha, \sin\alpha, 0)$ on the xy plane where α is the angle from the x-axis. The displacement field at any point $(r\cos\alpha, r\sin\alpha, 0)$ on the surface can be obtained from the value given in Figure 1 by dividing it by r since the displacement field varies as $1/r$. Figure 2 gives the stress field τ_{33}, or the traction vector T_3, as a function of $X1$ and $X3$ for points $(X1, 0{\cdot}5, X3)$ in a plane parallel to the xz plane. The origin is avoided because the displacement field is singular at the origin.

3.2. Tetragonal carbon-fiber composite

We take the c-axis of the tetragon along the x_3-direction. The results for an orthotropic solid reduce to the tetragonal case when we impose the following relations amongst the elastic constants. The numerical values given below are in units of c_{44} (= 25·9 GPa) for a graphite-epoxy composite containing 50% fibers by volume. These values were obtained by Heaton and quoted in [56, Chapter 5].

$$c_{55} = c_{44} = 1, c_{22} = c_{11} = 3{\cdot}1, c_{33} = 54{\cdot}6, c_{12} = 1{\cdot}2, c_{13} = c_{23} = 1{\cdot}9, c_{66} = 0{\cdot}7.$$

Figures 3 and 4 give the results for the tetragonal solid corresponding to Figures 1 and 2 described above.

3.3. Hexagonal carbon-fiber composite

We take the c-axis of the hexagon along the x_3-direction. The results given in Sec 3.2 for the tetragonal case reduce to hexagonal symmetry for $c_{66} = 0{\cdot}5(c_{11} - c_{12})$. The values given

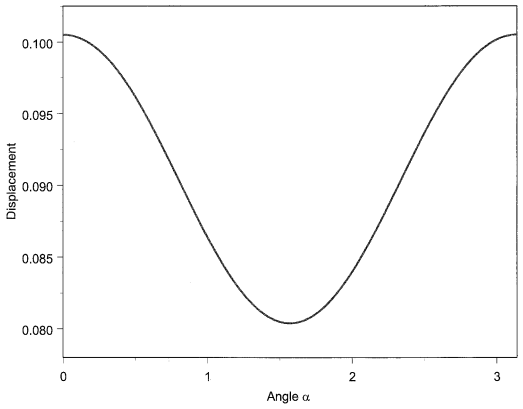

Figure 1. The z-component of the displacement field plotted as a function of α for points $(\cos\alpha, \sin\alpha, 0)$ at the free surface for PEEK. A normal load $(0,0,\eta_3)$ is applied at the origin. The units are such that $c_{44} = \eta_3 = 1$ (see Section 3). The angle α is measured from the x-axis and is in radians.

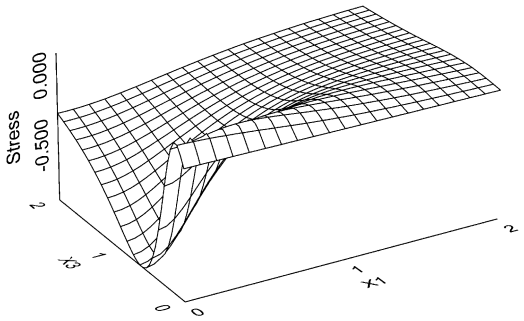

Figure 2. The z-component of the traction vector T3, or stress τ_{33}, plotted as a $X1$ and $X3$ for points $(X1,0{\cdot}5,X3)$ for PEEK. See Figure 1 for units.

below are for a graphite/epoxy composite containing 50% fibers by volume. These values were obtained by Heaton and quoted in [56, Chapter 5] in units of $c_{44} = 22{\cdot}7$ GPa.

$$c_{55} = c_{44} = 1, c_{22} = c_{11} = 1{\cdot}4, c_{33} = 19{\cdot}3, c_{12} = 0{\cdot}4, c_{13} = c_{23} = 0{\cdot}9.$$

Figure 5 shows the displacement field as a function of $X2$ for points $(X1, X2, 0)$ on the free surface of the hexagonal solid for two values $X1$. Since a hexagonal solid is transversely isotropic, the displacement field is independent of α defined in Figure 1. Figure 6 gives the results for the hexagonal solid corresponding to Figure 2 described above.

3.4. Single-crystal cubic silicon

The results for the tetragonal case reduce to cubic symmetry for $c_{11} = c_{22} = c_{33}, c_{44} = c_{55} = c_{66}$, and $c_{12} = c_{13} = c_{23}$. The numerical values of the elastic constants given below are for a single-crystal silicon in units of $c_{44} = 79{\cdot}6$ GPa, and have been taken from [8].

$$c_{44} = 1, c_{11} = 2{\cdot}1, c_{12} = 0{\cdot}8.$$

Figures 7 and 8 give the results for the cubic single-crystal silicon corresponding to Figures 1 and 2 described in Section 3.1.

3.5. Isotropic solid

The results for cubic symmetry reduce to those for isotropic solid if $c_{11} - c_{44} = 2c_{12}$. Our results for the isotropic case agree exactly with those given by Sneddon [24, Chapter 10] and, therefore, are not given here.

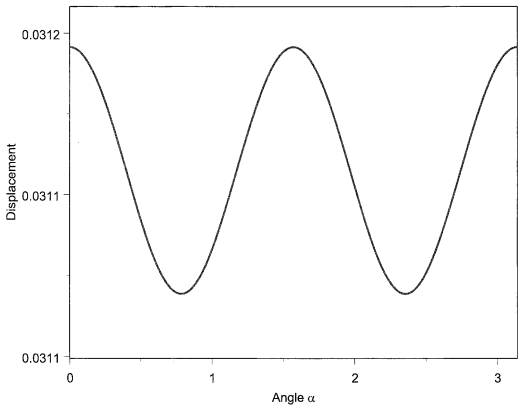

Figure 3. Same as Figure 1 for tetragonal carbon-fiber composite.

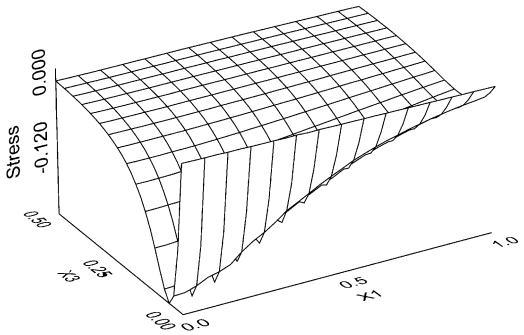

Figure 4. Same as Figure 2 for tetragonal carbon-fiber composite.

3.6. Discussion

The main features of the curves in the figures are summarized as follows. The variation of the displacement field with angle α on the free surface in Figures 1, 3, and 7 indicates anisotropy. The angular variation of the displacement field on the xy-plane as shown in Figures 3 and 7 is consistent with the rotational and reflection symmetry of the solid. Both tetragonal and cubic solids have this symmetry. This explains the periodicity of $\pi/4$ in the displacement field in Figure 3 for the tetragonal solid and Figure 7 for the cubic solid. For isotropic and transversely isotropic solids the displacement on the xy plane is independent of α. Figure 5 shows the expected $1/r$ dependence of the displacement field. The results for single-crystal silicon are relevant to formation and growth of arrays of quantum dots because the favorable location of the growth of a new quantum dot depends upon the strain field of the existing quantum dots [28].

Figures 2, 4, 6, and 8 show that the stress field τ_{33}, or the traction vector T_3, is zero at the free surface as required by the boundary condition, and approaches zero as $1/r^2$ for large r. This is the reason why the stress field τ_{33} must have at least one extremum (maximum or minimum) even for isotropic solids. Since the stress field varies as $1/r^2$ for large r for all solids, the extrema occur close to the free surface. The effect of anisotropy is particularly interesting for PEEK in Figure 2 that has two extrema. As is apparent from (2.4), the stress field depends upon the gradient of the displacement field in all the three directions and hence is quite sensitive to local anisotropy.

4. Conclusions

We have described a semi-analytical GF method based upon the delta-function representation for calculating displacement and stress fields in 3D anisotropic semi-infinite solids having one free surface and extending to infinity in other directions. The method is computationally efficient and applicable to arbitrary anisotropy. It gives analytical results for the even components of the Green's function at the free surface and requires only a 1D numerical integration over a finite interval at a general point in the solid. We have obtained numerical results for orthotropic PEEK carbon-fiber composite characterized by nine elastic constants, tetragonal carbon-fiber

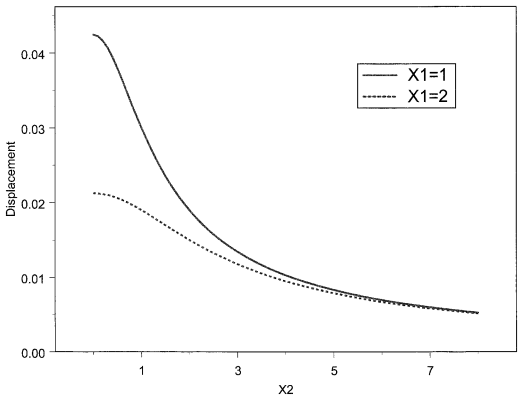

Figure 5. The z-component of the displacement field plotted as a function of $X2$ for points $(X1, X2, 0)$ for hexagonal carbon-fiber composite. See Figure 1 for units.

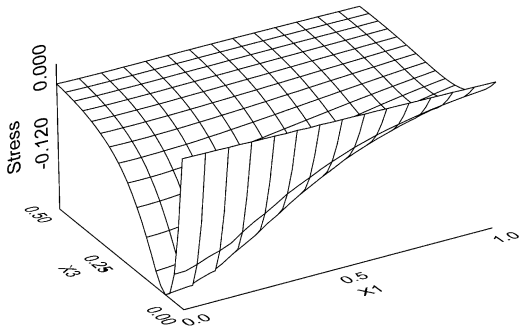

Figure 6. Same as Figure 2 for hexagonal carbon-fiber composite.

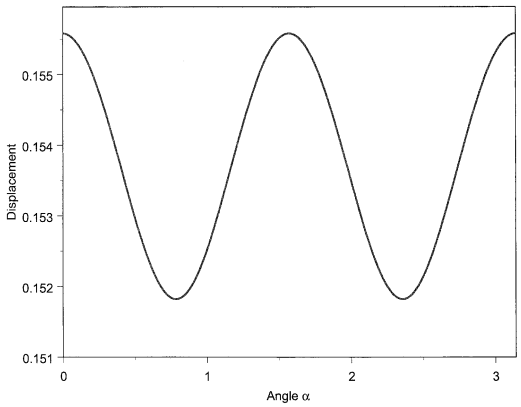

Figure 7. Same as Figure 1 for single crystal cubic silicon.

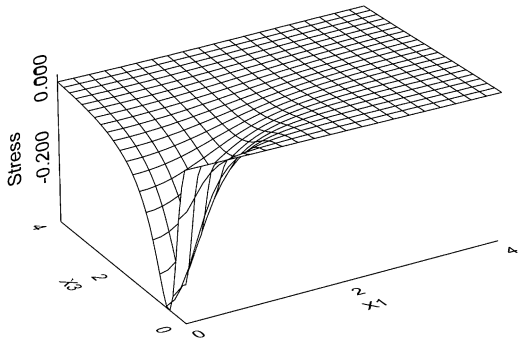

Figure 8. Same as Figure 2 for single crystal cubic silicon.

composite characterized by 6 elastic constants, a transversely isotropic hexagonal fiber composite characterized by 5 elastic constants, and a cubic silicon single crystal characterized by 3 elastic constants. These results should be useful for application to the BEM analysis of these materials, interpretation of nanoindentation measurements, and calculation of stress fields in silicon caused by the presence of a quantum dot at the free surface.

Acknowledgements

I thank Drs. Colm Flannery and Tim Quinn for reading this manuscript and their useful comments and suggestions. This work was supported in part by the NIST Advanced Technology Program.

Appendix A. Integration of the Green's function in the reciprocal space

We give the evaluation of the integral in (2.14) in the case when the roots of the determinantal equation are complex. For a detailed and rigorous analysis of generalized functions, see, for example, [57, Chapter III]. Consider the following integral involving the Dirac delta function

$$I = \int_C \delta[F(y)]\Phi(y)\mathrm{d}y, \tag{A1}$$

where the integration is over a contour C in the complex plane, $\Phi(y)$ is an integrable function, and $F(y)$ is real. If the integration is over the real axis and $F(y) = 0$ has real roots, the integral can be evaluated by using the standard formula for the delta function of a function expressed in terms of the delta function of the roots.

For complex roots we deform the contour to include $F(y) = 0$ and transform the integration variable in (A.1) from y to z, where

$$z = F(y), \tag{A2}$$

$$\mathrm{d}y = \mathrm{d}z/F'(y), \tag{A3}$$

and the prime over F denotes its derivative with respect to y. From (A.1)

$$I = \int \delta(z)\Phi[y(z)]\mathrm{d}z/F'[y(z)]. \tag{A4}$$

where the integration is over the real axis including the point z =0. This gives

$$I = \Phi[y(z=0)]/F'[y(z=0)]. \tag{A5}$$

If $y = b$ is a real or complex root of $F(y) = 0$, then

$$y(z=0) = b. \tag{A6}$$

Using (A.6) in (A.5) gives the value of the integral. If $F(y) = 0$ has multiple roots, we need to sum the right hand side of (A.5) over the roots as given below. Thus, in (A.1), we choose C such that the integral over z includes the point $z = 0$.

If $F(y)$ is an Nth-degree polynomial in y with real or complex roots y_m where $m = 1, 2 \ldots N$, we can write

$$F(y) = C \prod_{m=1,N} (y - y_m), \tag{A7}$$

where C is the coefficient of y^N in the polynomial. Using (A.7) in (A.5),

$$I = \sum_m \Phi[y_m]W_m, \tag{A8}$$

$$W_m = [\partial F(\mathbf{y})/\partial y_m]^{-1} = 1/[C \prod_{m' \neq m} (y_m - y_{m'})]. \tag{A9}$$

The determinant $D(\boldsymbol{q})$ in (2.13) is a 6-degree polynomial in q_i or a cubic polynomial in q_i^2 in certain symmetry directions. We write it as a polynomial in q_3 as follows

$$D(Q, q_3) = C \prod_{m=1,6} (q_3 - q_{3m}), \tag{A10}$$

where C is the coefficient of q_3^6 in $D(q_3)$ and q_{3m} (m = 1-6) are the six roots of the equation

$$D(Q, q_3) = 0. \tag{A11}$$

Since D is real, the roots q_{3m} are in general complex and will occur in complex conjugate pairs. The roots will be functions of $\boldsymbol{Q}$ or θ. Using (A.8–A.10), we obtain the following formula for the integral over q_3 for any integrable function $\Phi(\boldsymbol{q})$:

$$\begin{aligned} \int \delta[D(\boldsymbol{q})]\Phi(\boldsymbol{q}) dq_3 &= \int \delta[D(\mathbf{Q}, q_3)]\Phi(\mathbf{Q}, q_3) \mathrm{d}q_3 \\ &= \sum_m \Phi[\mathbf{Q}, q_{3m}] W_m, \end{aligned} \tag{A12}$$

where

$$W_m = 1/[C \prod_{m', \neq m} (q_{3m} - q_{3m'})]. \tag{A13}$$

Equation (A.12) leads to (2.21) and (2.22). In view of (2.8), we include only the three roots with positive imaginary parts in the sum in (A.12) for $x_3 > 0$. All the six roots must be included (except $m' = m$) in the product in (A.13), so we take m = 1-3 and m'= 1-6. The degenerate cases can be handled by the method suggested by Ting and Lee [12] or by making the elastic constants slightly different so as to lift degeneracy.

Appendix B. Determination of the virtual force

We use the delta function of a vector variable and solve (2.18) for the virtual force. The delta function of a 2D vector variable $\boldsymbol{X}$ is defined in terms of its Cartesian components X_1 and X_2as follows:

$$\delta(\boldsymbol{X}) = \delta(X_1)\delta(X_2). \tag{B1}$$

In the Fourier representation

$$\delta(\boldsymbol{X}) = (1/2\pi)^2 \int \int_{-\infty}^{\infty} \exp(\mathrm{i}\boldsymbol{K}\cdot\boldsymbol{X}) \mathrm{d}K_1 \mathrm{d}K_2, \tag{B2}$$

where $\boldsymbol{K}$ is a 2D vector with Cartesian components K_1 and K_2. In polar coordinates, (B.2) becomes

$$\delta(\boldsymbol{X}) = (1/2\pi)^2 \int_0^{\infty} \int_0^{2\pi} \exp[\mathrm{i}KX\cos(\varphi)] K \mathrm{d}K \mathrm{d}\varphi, \tag{B3}$$

where $\boldsymbol{K}$ and $\boldsymbol{X}$ are magnitudes of $\boldsymbol{K}$ and $\boldsymbol{X}$, respectively, and φ is the polar angle.

We use (B.3) to prove the following relation:

$$\int_0^{2\pi} \Delta'(\boldsymbol{Q}\cdot\boldsymbol{X})\mathrm{d}\varphi = -4\pi\delta(\boldsymbol{X}), \tag{B4}$$

where the function Δ has been defined in (2.8) and the prime over Δ denotes its derivative with respect to its argument.

We write (2.8) in the integral representation as follows:

$$\Delta(z) = (\mathrm{i}/\pi)\int_0^{\infty} \exp[\mathrm{i}\omega z]\mathrm{d}\omega, \tag{B5}$$

Differentiating both sides of (B.5) with respect to z, we obtain for $z = \boldsymbol{Q}\cdot\boldsymbol{X}$

$$\int_0^{2\pi} \Delta'(\boldsymbol{Q}\cdot\boldsymbol{X})\mathrm{d}\varphi = -(1/\pi)\int_0^{\infty} \omega\mathrm{d}\omega \int_0^{2\pi} \exp[\mathrm{i}\omega X\cos\varphi]\mathrm{d}\varphi, \tag{B6}$$

where we have written $\boldsymbol{Q}\cdot\boldsymbol{X} = X\cos\varphi$ since $\boldsymbol{Q}$ is a unit vector. From (B.3) and (B.6), we obtain (B.4). The solution of (2.18) is then given by (2.21), which can be verified by direct substitution.

References

1. D. Bimberg, M. Grundmann and N.N. Ledentsov, *Quantum Dot Heterostructures.* New York: John Wiley (1999) 328pp.
2. M. Hebbache and M. Zemzemi, Nanoindentation of silicon and structural transformation: Three-dimensional contact theory. *Phys. Rev. B* 67 (2003) article number 233302.
3. T.A. Cruse, *Boundary-element Analysis in Computational Fracture Mechanics.* Dordrecht: Kluwer Academic Publishers (1988) 162pp.
4. A.G. Every and K.Y. Kim, Determination of elastic constants of anisotropic solids from elastodynamic Green's Functions. *Ultrasonics* 34 (1996) 471–472.
5. T. Dutta, T.K. Ballabh and T.R. Middya, Green-Function calculation of effective elastic constants of polycrystalline materials. *J. Phys. D-Appl. Phys.* 26 (1993) 667–675.
6. R. Arias, Elastic fields of stationary and moving dislocations in finite samples. *Phil. Mag. B* 78 (1998) 109–113.
7. T.C.T. Ting and D.M. Barnett, Image force on line dislocations in anisotropic elastic half-spaces with a fixed boundary. *Int. J. Solids Struct.* 30 (1993) 313–323.
8. J.P.Hirth and J. Lothe, *Theory of Dislocations.* Malabar, Florida: Kreiger Publishing Company (1992) 857pp.
9. V.K. Tewary, Multiscale Green's-function method for modeling point defects and extended defects in anisotropic solids: application to a vacancy and free surface in copper. *Phys. Rev. B* (2004) article number 094109.
10. T.C.T. Ting, *Anisotropic Elasticity: Theory and Applications.* New York: Oxford University Press (1996) 570pp.
11. T. Mura, *Microechanics of Defects in Solids.* The Hague: Martinus Nijhoff Publishers (1982) 494pp.
12. T.C.T. Ting and V.G. Lee, The three-dimensional elastostatic Green's function for general anisotropic linear elastic solids. *Q. J. Mech. Appl. Math.* 50 (1997) 407–426.
13. D.M. Barnett, The precise evaluation of derivatives of the anisotropic elastic Green's functions. *Physica Status Solidi (b)* 49 (1972) 741–748.
14. J.W. Deutz and H.R. Schober, Boundary value problems using elastic Green's functions. *Comp. Phys. Comm. (Netherlands)* 30 (1983) 87–91.
15. S.A. Gunderson and J. Lothe, A new method for numerical calculations in anisotropic elasticity problems. *Physica Status Solidi (b)* 143 (1987) 73–85.
16. Y. Hisada, Efficient method for computing green's functions for a layered half-space with sources and receivers at close depths. *Bull. Seismolog. Soc. Am.* 85 (1995) 1525–1526.

17. E. Pan, Static green's functions in multilayered half spaces. *Appl. Math. Modell.* 21 (1997) 509–521.
18. T.C.T. Ting, Green's functions for an anisotropic elliptic inclusion under generalized plane strain deformations. *Q. J. Mech. Appl. Math.* 49 (1996) 1–18.
19. E. Pan and F.G. Yuan, Three-dimensional Green's functions in anisotropic bimaterials. *Int. J. Solids Struct.* 37 (2000) 5329–5351.
20. C.Y. Wang, 2-Dimensional elastostatic Green's Functions for general anisotropic solids and generalization of Stroh's Formalism. *Int. J. Solids and Struct.* 31 (1994) 2591–2597.
21. C.Y. Wang and J.D. Achenbach, A new method to obtain 3-D Green's functions for anisotropic solids. *Wave Motion* 18 (1993) 273–289.
22. C.Y. Wang, Elastic fields produced by a point source in solids of general anisotropy. *J. Engng. Math.* 32 (1997) 41–52.
23. J.R. Willis, Self-similar problems in elastodynamics. *Phil. Trans. R. Soc.* A274 (1973) 435–491.
24. I.N. Sneddon, *Fourier Transforms.* New York: McGraw Hill (1951) 542 pp.
25. E. Pan and B. Yang, Elastostatic fields in an anisotropic substrate due to a buried quantum dot. *J. Appl. Phys.* 90 (2001) 6190–6196.
26. E. Pan, Three-dimensional Green's functions in an anisotropic half space with general boundary conditions. *J. Appl. Mech.-Trans. ASME* 70 (2003) 101–110.
27. K.P. Walker, Fourier integral representation of the Green function for an anisotropic elastic half-space. *Proc. R. Soc., London A* 443 (1993) 367–389.
28. B. Yang and V.K. Tewary, Formation of a surface quantum dot near laterally and vertically neighboring dots. *Phys. Rev. B* 68 (2003) article number 035301.
29. H. Hasegawa, V.G. Lee and T. Mura, Green-functions for axisymmetrical problems of dissimilar elastic solids. *J. Appl. Mech.-Trans. ASME* 59 (1992) 312–320.
30. R. Rajapakse and Y. Wang, Greens-functions for transversely isotropic elastic half-space. *J. Engng. Mech.-ASCE* 119 (1993) 1724–1746.
31. I.N. Sneddon, Fourier-transform solution of a boussinesq problem for a hexagonally aeolotropic elastic half-space. *Q. J. Mech. Appl. Math.* 45 (1992) 607–616.
32. H.Y. Yu, S.C. Sanday and C.I. Chang, Elastic inclusions and inhomogeneities in transversely isotropic solids. *Proc. R. Soc. London A* 444 (1994) 239–252.
33. Z.Q. Yue, Closed-form Green's functions for transversely isotropic bi-solids with a slipping interface. *Struct. Engng. Mech.* 4 (1996) 469–484.
34. R.Y.S. Pak and F. Ji, Axisymmetrical stress-transfers from an embedded elastic cylindrical-shell to a half-space. *Proc. R. Soc. London A* 441 (1993) 237–259.
35. M.A. Sales and L.J. Gray, Evaluation of the anisotropic Green's function and its derivative. *Comp. Struct.* 69 (1998) 247–254.
36. Y.C. Pan and T.W. Chou, Point force Solution for an infinite transversely isotropic solid. *J. Appl. Mech.-Trans. ASME* 43 (1976) 608–612.
37. Y.C. Pan and T.W. Chou, Green's function solutions for semi-infinite transversely isotropic materials. *Int. J. Engng. Sci.* 17 (1979) 545–551.
38. Y.C. Pan and T.W. Chou, Green's functions for two-phase transversely isotropic materials. *J. Appl. Mech.-Trans. ASME* 46 (1979) 551–556.
39. C.D. Wang, C.S. Tzeng, E. Pan, J.J. Liao, Displacements and stresses due to a vertical point load in an inhomogeneous transversely isotropic half-space. *Int. J. Rock Mech. Mining Sci.* 40 (2003) 667–685.
40. D.M. Barnett and J. Lothe, Line force loadings on anisotropic half-spaces and wedges. *Physica Norvegica* 8 (1975) 13–22.
41. J.R. Barber, Some polynomial solutions for the non-axisymmetric boussinesq problem. *J. Elasticity* 14 (1984) 217–221.
42. E. Pan and F.G. Yuan, Boundary element analysis of three-dimensional cracks in anisotropic solids. *Int. J. Num. Meth. Engng.* 48 (2000) 211–237.
43. F. Tonon, E. Pan and B. Amadei, Green's functions and boundary element method formulation for 3D anisotropic media. *Comp. Struct.* 79 (2001) 469–482.
44. M. Gellert, Discrete numerical-solution of the generalized Boussinesq problem. *Int. J. Num. Meth. Engng.* 21 (1985) 2131–2144.
45. J.R. Willis, Hertzian contact of anisotropic bodies. *J. Mech. Phys. Solids* 14 (1966) 163–176.

46. A.G. Every, Displacement field of a point force acting on the surface of an elastically anisotropic half-space. *J. Physics A* 27 (1994) 7905–7914.
47. V.K. Tewary, Computationally efficient representation for elastodynamic and elastostatic Green's functions for anisotropic solids. *Phys. Rev.* B51 (1995) 15695–15702.
48. P.M. Morse and H. Feshbach, *Methods of Mathematical Physics: Part I.* New York: McGraw-Hill (1953) 1037pp.
49. V.K. Tewary, R.H. Wagoner and J.P. Hirth, Elastic Green's function for a composite solid with a planar interface. *J. Materials Res.* 4 (1989) 113–123.
50. V.K. Tewary, Elastic Greens-function for a bimaterial composite solid, containing a free-surface normal to the interface. *J. Materials Res.* 6 (1991) 2592–2608.
51. P.A. Martin, On Green's function for a biomaterial elastic half-plane. *Int. J. Solids Struct.* 40 (2003) 2101–2119.
52. L. Pan, *Boundary-Element Strategies and Discretzied Green's Functions.* Ph.D. Thesis, Iowa State University (1997) 156pp.
53. P.A. Martin and F.J. Rizzo, Partitioning, boundary integral equations, and exact Green's functions. *Int. J. Num. Meth. Engng.* 38 (1995) 3483–3495.
54. V.K. Tewary, M. Mahapatra and C.M. Fortunko, Green's function for anisotropic half-space solids in frequency space and calculation of mechanical impedance. *J. Acoust. Soc. Am.* 100 (1996) 2960–2963.
55. K.Y. Kim, T. Ohtani, A.R. Baker and W. Sachse, Determination of all elastic constants of orthotropic plate specimens from group velocity data. *Res. Nondestruct. Eval.* 7 (1995) 13–29.
56. V.K. Tewary, *Mechanics of Fiber Composites.* New York: John Wiley (1979) 288pp.
57. I.M. Gel'fand and G.E. Shilov, *Generalized functions – Vol 1.* New York: Academic Press (1964) 423 pp.